



Open
Access

A Computational Fluid Dynamics Study of an Integrating Savonius-Darrieus Vertical Axis Wind Turbine

Abdel-Fattah Mahrous^{1,2,*}

¹ Mechanical Engineering Department, College of Engineering, Taif University, P.O. Box 888, Taif, Saudi Arabia

² Mechanical Power Engineering Department, Faculty of Engineering, Menoufia University, 32511, Shebin El-Kom, Egypt

ARTICLE INFO

Article history:

Received 20 December 2019

Received in revised form 5 April 2020

Accepted 1 May 2020

Available online 3 September 2020

ABSTRACT

To combine the advantages of performance of both Savonius and Darrieus wind turbines, this paper aims to study computationally a novel design configuration of a Vertical Axis Wind Turbine (VAWT). The new design would help cover a broad range of performance parameters between both types of wind turbines as well as overcome drawbacks of the Savonius type at higher rotational speed. The proposed design is to integrate both of Savonius and straight blade Darrieus wind turbines in a single VAWT design configuration. In this design, the turbine rotor consists of a number of similar NACA0015 airfoil blades set in a particular arrangement. By regulating individual angles of rotor blades, the turbine would work as either Savonius or H-Darrieus VAWT. The turbine could also be set to work at different configurations between those for the Savonius and H-Darrieus ones. The computational results revealed that the performance of the proposed integrating wind turbine would be controlled and optimized to cover the operating range of both of Savonius and Darrieus wind turbines. Besides, the performance of Savonius VAWT would be modified when applying this design. When the proposed design is practically implemented, characteristics of both of Savonius and H-Darrieus based wind turbines would be found in a single design.

Keywords:

Vertical axis wind turbines; Savonius; H-Darrieus; integrating design; computational study

Copyright © 2020 PENERBIT AKADEMIA BARU - All rights reserved

1. Introduction

With the dramatic increase in global populations and limitations in natural resources of energy, looking for alternative energy resources to compensate increasing demand of electricity becomes a necessity. Renewable energy resources, such as wind, solar and hydro power, receive a great attention as clean energy sources.

Wind turbines have been extensively used throughout the world to generate electricity from wind power. There are two main types of wind turbines according to the disposition of turbine shaft. These are the Horizontal Axis Wind Turbines (HAWT) and the Vertical Axis Wind Turbines (VAWT). In the

* Corresponding author.

E-mail address: afmahrous@yahoo.com

HAWT, the blades rotating axis is parallel to the wind stream. The advantages of HAWT include high turbine efficiency and high-power density. On the other hand, blades of the VAWT rotate with respect to a vertical axis that is perpendicular to the ground level as well as wind stream. An important feature of the VAWT is that it accepts wind from any direction (i.e. independence of wind direction) and therefore no yaw mechanism is required. Savonius (drag type) and Darrieus (lift type) wind turbines are the main types of VAWT.

The two types of VAWT are shown in Figure 1 [1]. The Savonius type VAWT, Figure 1(a), is a simple machine having two (or more) half-cylindrical parts attached to opposite sides of a vertical shaft. It is considered as a drag type wind turbine as the incoming wind stream drags/pushes the rotor blades (or buckets) causing them to rotate around the vertical shaft. The drag force on the concave or advancing bucket (blade moving in the direction of the wind) is higher than that on the convex or returning bucket (blade moving against the wind) causing a net force that can drive the rotor. The Darrieus type VAWT, Figure 1(b) and Figure 1(c), is provided with two or more airfoil-shaped blades mounted on a vertical shaft. The rotor blades are either bent (egg bladder type) or straight (H-type). The energy is extracted from the wind mainly through an aerodynamic lift force that is working in the direction of rotation. The aerodynamic lift force is created when the wind is blowing over the airfoil profile of the rotor blade and, thus, this type of VAWT is called lift driven VAWT. When compared with drag force based VAWT, using lift force based VAWT results in production of much power as well as turbine rotor can acquire higher rotational speed.

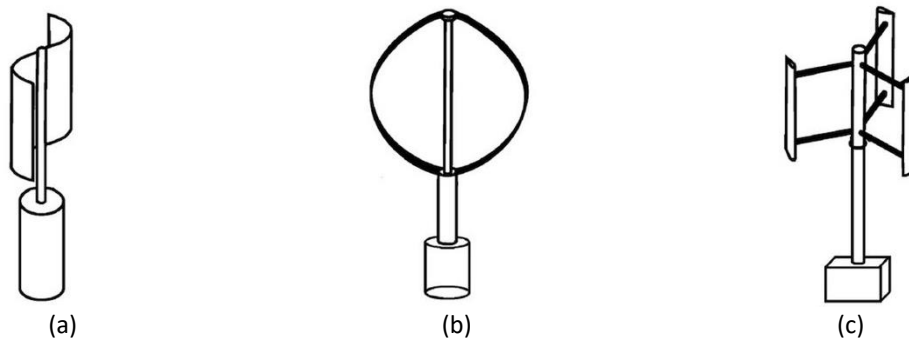


Fig. 1. Rotors of VAWT turbines: (a) Savonius; (b) Darrieus; (c) H-Darrieus [1]

Much research has been carried out so far in order to improve VAWT performance and to maximize the energy generation from the available wind power. In the case of Savonius type VAWT, this was done by considering alternate turbine designs such as twisting and/or modifying profiles of rotor blades [2-7], adding a fixed shielding plates, wind boosters or curtains (or ducts) around the entry of wind turbine to enhance wind power [8-10] as well as by increasing the number of rotor blades [11-12] or number of stages (i.e. multi step rotors) [13-14]. In a wind farm of Savonius wind turbines, managing the location of individual wind turbines can help optimizing the overall output power. Proper location of downstream turbines can be estimated by using velocity pattern analysis to identify zones of strongest vortices [15]. Augmentation of the power output of an H-Darrieus rotor by using a flat plate deflector was investigated by Wong *et al.*, [16]. The effect of number of blades on the performance of VAWT was studied in references [11-12] and [17]. Furthermore, an attempt was made to design a hybrid turbine of Darrieus and a double/multi step Savonius turbine coupled on a single shaft and tested in different currents [14, 18-19]. However, applying either the Savonius or the Darrieus based VAWT alone or in a hybrid configuration may not entirely satisfy the required energy envelope.

The theoretical power coefficient, C_p , (as a measure of wind turbine efficiency) versus tip speed ratio, λ , for various configurations of common wind turbine designs is shown in the Figure 2 [20]. Tip speed ratio is the ratio between rotor blades tip speed and wind speed. The theoretical maximum efficiency of a wind turbine, given by the Betz Limit [21], is about 59%. As can be seen, the HAWTs are the most efficient with a power coefficient of about 0.49. However, HAWTs operate only at higher values of tip speed ratio. Despite the lower power coefficient of VAWTs (Savonius for example), they can operate at lower values of tip speed ratio. Owing to lower power output, VAWT has currently been paid a great attention in research. A maximum power coefficient of about 0.4 can be achieved by the Darrieus type VAWT turbine with a tip speed ratio range approximately from 3.5 to 7.5. On the other hand, Savonius design wind turbine can achieve a maximum power coefficient of about 0.14 with a tip speed ratio less than 1.5. Through the tip speed ratio operating range of VAWT (0.0: 7.5), Savonius VAWT is the most efficient at lower values of tip speed ratio while Darrieus VAWT works more efficiently at higher values of tip speed ratio. In order to take the advantages of both VAWTs designs, and to cover the operating range of tip speed ratio between them, an integrating design (not a hybrid or combination) of both of Savonius and Darrieus concepts is essential and demanding. Rotors of the new design would have adjustable blades to cover the performance curves from Savonius to Darrieus wind turbines and vice versa. This means switching between both designs would be achieved by adjusting blade angles.

The main objective of the present work was to computationally study a novel design of VAWT combines the features of both Savonius and Darrieus wind turbines in a single configuration. The proposed design is an integrating design of both of Savonius and straight blade Darrieus (H- Darrieus) wind turbines that, when developed, would operate in a wide range of tip speed ratio and with optimum power output.

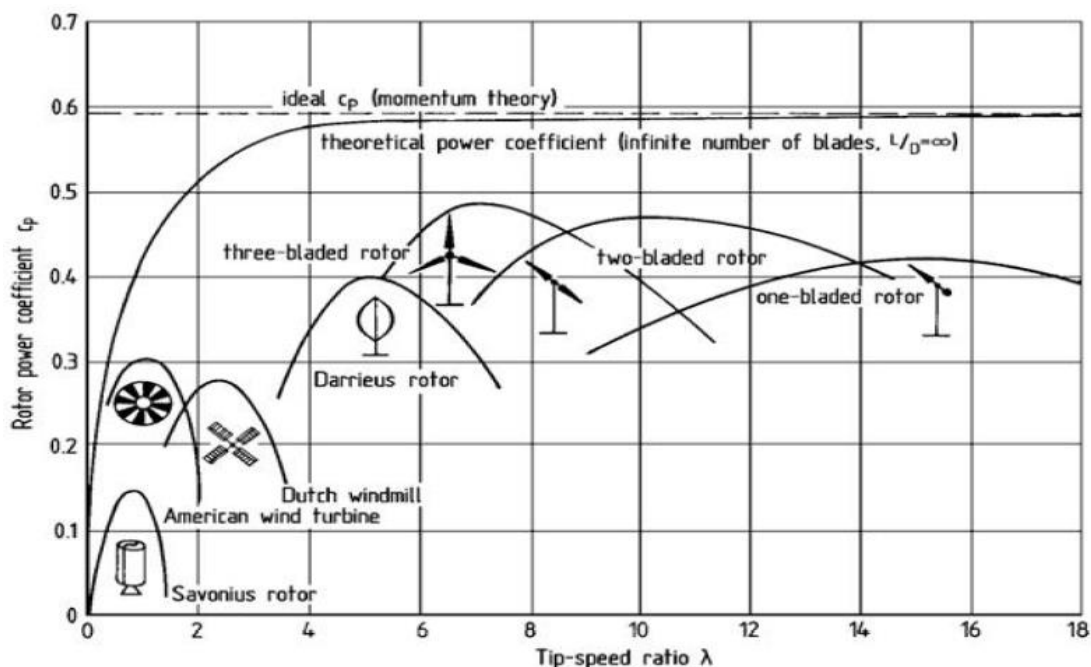


Fig. 2. Power coefficient versus tip speed ratio for a variety of turbine configurations [20]

2. Proposed Design Configuration of Savonius-Darrieus Integrating Wind Turbine Rotor

Rotor blades of the proposed design, depicted in Figure 3, are of NACA0015 [22] straight airfoil. NACA0015 airfoils are widely used as H-Darrieus airfoil blades [23]. The NACA0015 airfoil is

symmetrical with no camber. The number 15 means that the airfoil has a 15% thickness to chord length. The airfoil blades, with chord length of 148mm, are pivot on a half circular arc (blades' circle) at 1/4 of the chord distance from the leading edge, see Figure 4. The blades are positioned on the semicircular arc such that the angle between the pivots of two consecutive blades, measured from the center of the arc (blades' circle), is 30°.

Resembling an S-shape, two half circular arcs with the arrangement of blades shown in Figure 4 are used to form the wind turbine rotor. By closing the flow passages between successive blades through the rotation about pivots in anticlockwise direction, an approximate C-arc is formed resulting in a Savonius type VAWT (State 1 in Figure 5(a)). On the other hand, a Darrieus type is formed with the flow passages being fully open (State 5 in Figure 5(e)). Flow passage is considered fully open when chords lines of action of rotor blades are parallel to each other.

Between the two states of rotor blades mentioned so far (i.e. State 1 and State 5 in Figure 5(a) and Figure 5(e), respectively), the rotor blades can individually be adjusted at the required adjustment angle in order to control the turbine output power. Blades are adjusted, for instance, in such a way that they are set at 25%, 50% and 75% of their full range of adjustment between the two main states of Savonius and Darrieus states, see Figure 5(b), 5(c), and 5(d). This can be practically accomplished by using position control applied on an appropriate electric motor either stepper motor or the well-known induction motor. The utilized motor has a small rating power and it is controlled based on measured wind speed. The monitored wind speed is used as an input to the motor drive and is categorized into several speed ranges that depend on the investigated states of rotor blades.

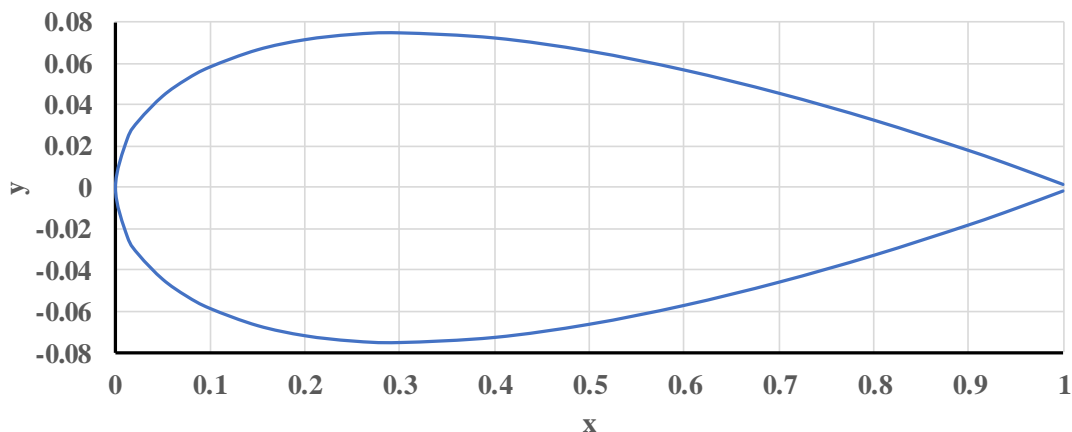


Fig. 3. NACA0015 blade configuration [22]

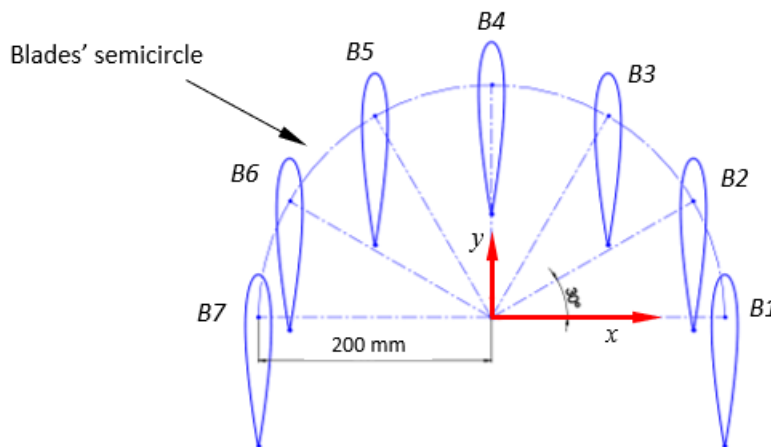


Fig. 4. Arrangement of NACA0015 airfoil blades on a part of the proposed turbine rotor

Accordingly, the investigated states of integrating wind turbine rotor blades are the 0% (Savonius), 25%, 50%, 75% and 100% (Darrieus) of full blades' range of adjustment about their pivots in clockwise direction. It should be noted that the angle of full range of adjustment between Savonius and Darrieus states differs from one blade to another, see Table 1. To switch from Darrieus based VAWT back to Savonius VAWT, rotor blades should be regulated about their pivots in counterclockwise direction. A one more state configuration of rotor blades is also investigated (State 6 in Figure 5(f)) where blades' chord lines are perpendicular to their corresponding radial arms drawn to pivots. In all cases (or rotor blades configurations) under investigation, the rotor outermost blades are kept fixed with respect to their pivots but rotates due to wind with other blades. The different states of turbine rotor blades illustrated in Figure 5 are at zero-degree angle of rotation, i.e. $\theta = 0.0$. Blowing the wind over the rotor blades will cause rotation of turbine rotor about its center in anticlockwise direction. Direction of rotation is shown for State 1 of Figure 5(a).

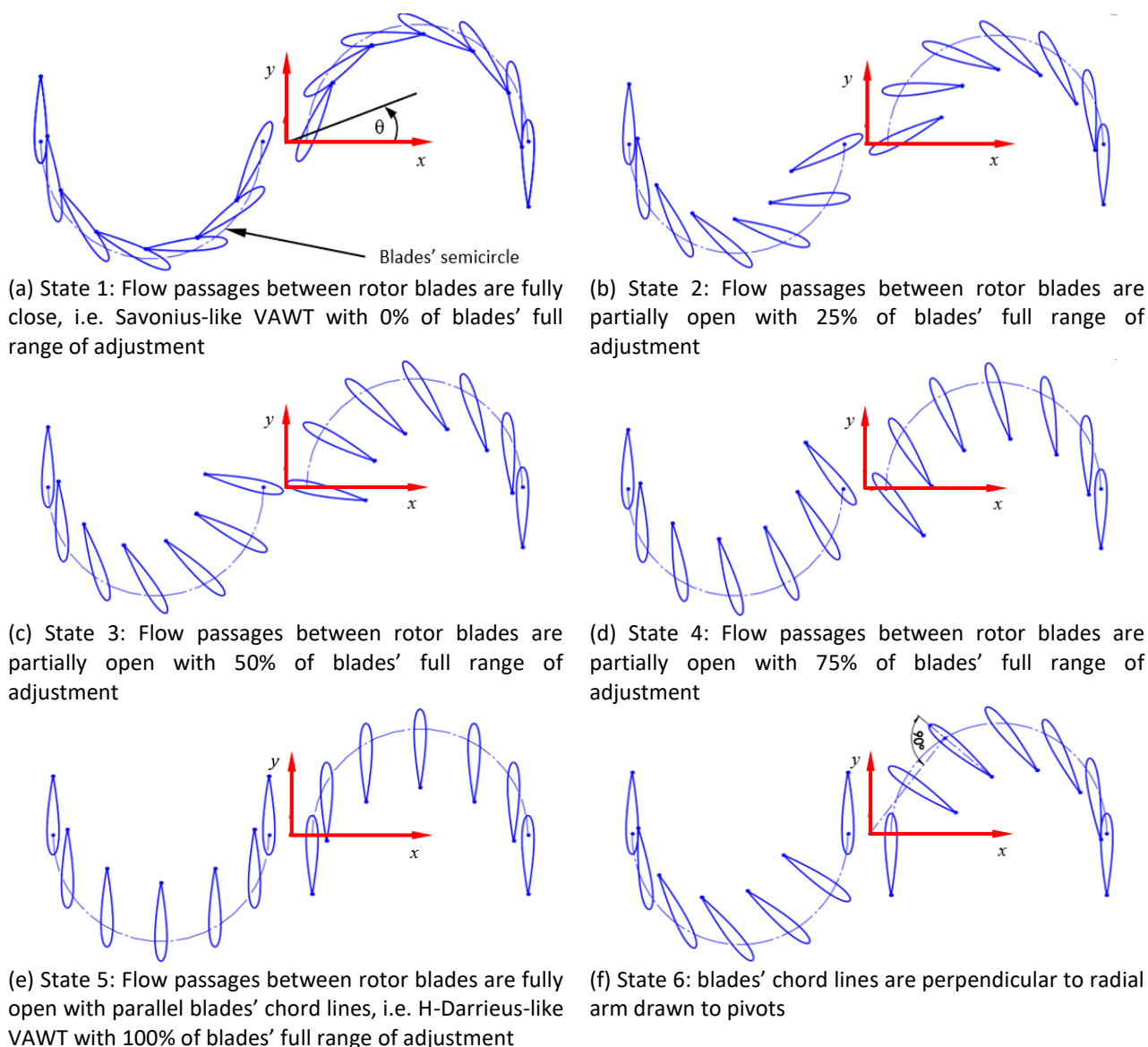


Fig. 5. Investigated states of rotor blades configuration for the proposed Savonius-Darrieus Integrating Vertical Axis Wind Turbine. Percentage shown denotes how much the blade angle of regulation is with regards to its full range of regulation

Table 1

Range of angle of regulation for airfoil rotor blades between Savonius and Darrieus states

Blade	B1	B2	B3	B4	B5	B6	B7
Range of adjustment (deg)	0°	8.05°	35.5°	65.07°	95°	125°	155°

3. Governing Equations and Computational Method

The performance of Savonius-Darrieus integrating vertical axis wind turbine was computationally calculated using a finite volume Computational Fluids Dynamics (CFD) solver, ANSYS Fluent 15. The governing equations of the fluid flow (air) throughout the turbine rotor are the mass and momentum conservation equations. The flow regime considered in the present study was turbulent and the problem was solved as two-dimensional flow. The governing equations of mass and momentum (Reynolds-Averaged Navier-Stokes (RANS) equations) are written in unsteady state condition as follows [24]:

$$\frac{\partial \rho}{\partial t} + \frac{\partial}{\partial x_j} (\rho u_j) = 0 \quad (1)$$

$$\frac{\partial}{\partial t} (\rho u_j) + \frac{\partial}{\partial x_i} (\rho u_i u_j) = -\frac{\partial P}{\partial x_j} + \rho g_j + \frac{\partial}{\partial x_i} \left[\mu \left(\frac{\partial u_i}{\partial x_j} + \frac{\partial u_j}{\partial x_i} \right) \right] + \frac{\partial}{\partial x_i} (-\overline{\rho u_i' u_j'}) \quad (2)$$

where ρ is the fluid density, t denotes the time, u_j is the velocity component in the direction j , P is the pressure, g is the acceleration due to gravity, μ is the molecular viscosity coefficient and x_i stands for spatial coordinate.

The last term in the momentum equation (Eq. (2)) represents the Reynolds shear stress tensor and it has to be modeled appropriately. Using the concept of turbulent viscosity, the Reynolds shear stress in Eq. (2) may be written as:

$$-\overline{\rho u_i' u_j'} = \mu_t \left(\frac{\partial u_i}{\partial x_j} + \frac{\partial u_j}{\partial x_i} \right) \quad (3)$$

The turbulent viscosity μ_t in Eq. (3) is computed using an appropriate turbulence model. In the present computational analysis, a two-equation turbulence model is used to determine the turbulent viscosity. Among the two-equation turbulence models, the k - ϵ turbulence model, proposed by Launder and Spalding [25], is most often used for turbulence predictions.

The computational domain is shown in Figure 6 with the appropriate boundary conditions. The arbitrary chosen dimensions of the turbine rotor, according to the literature available, are such that the radius of Savonius central C-arc (blades' semicircle radius) is of 200 mm while the rotor diameter (D) has been set to 908 mm. The domain has an upstream distance of 8000 mm (i.e. 9D) and a downstream distance of 25000 mm (i.e. 28D). Upper and lower symmetrical planes were set at 8000 mm each (i.e. 9D) from the turbine center. The computational domain is divided into two distinct zones: the rotating and stationary zones. Rotating zone is of 1600 mm diameter (i.e. 1.8D) and it was set around the turbine blades, while the stationary zone was assigned to the remaining part of the CFD domain. Interfaces were set at the surfaces separating the rotating and stationary zones. Sliding mesh concept [24] was applied to model rotating zone of the wind turbine. The rotating zone could rotate at different rotational speeds while the other zone was kept stationary. A uniform inlet fluid velocity profile of 10 m/sec and with a 5% turbulence intensity was imposed at the inlet boundary of

the computational domain, while a pressure outlet boundary condition of 1 standard atmosphere was assigned at the outlet section.

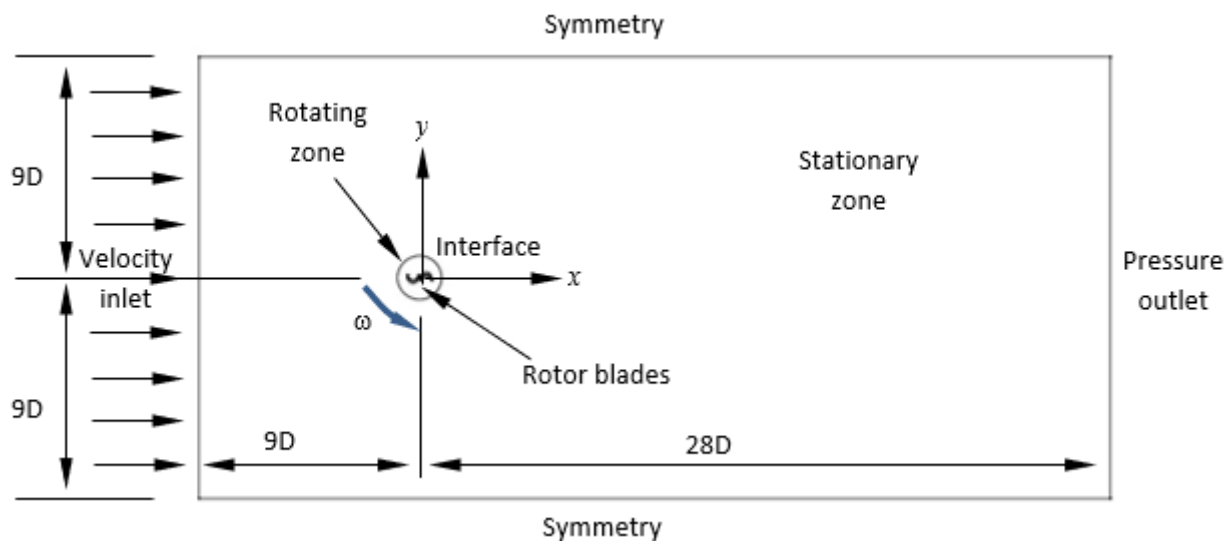


Fig. 6. 2-D Computational domain with boundary conditions. Rotating zone has a diameter of 1.8D

SolidWorks CAD software was used for building and exporting the 2-D geometry of the wind turbine test models. Having the geometry created in SolidWorks environment, it was imported into ANSYS Meshing and then discretized to create a 2-D mesh. The mesh has to be fine close to and in the vicinity of rotor blades. This helps in capturing all physical effects within the rotating zone and also in getting proper values for turbine performance parameters. The grid growth rate was set as 1.15. For the far field, flow may hardly be influenced by the wind turbine and consequently a coarser mesh was applied. Figure 7 shows the computational grid for the Darrieus-based integrating wind turbine as an example of turbine rotor test models. Triangular mesh was assigned to the rotating zone while a quad-tri hybrid mesh was chosen for the stationary zone.

To have a better relation between pressure and velocity, the SIMPLE algorithm (stands for Semi-Implicit Method for Pressure-Linked Equation) was chosen during the simulations. The SIMPLE algorithm uses a relationship between velocity and pressure corrections to enforce mass conservation and to obtain the pressure field [24]. Second order upwind discretization in momentum and time was applied throughout the calculations with double precision pressure-based algorithm. The transient time step of the rotor corresponds to 1° of rotation for any turbine angular velocity ($\Delta t = \pi / 180\omega$, where ω is the turbine angular velocity in rad/sec). This value of time step was considered to give time step solution independent [7]. In addition to the CFD conditions mentioned so far, no-slip conditions for the velocity components and zero normal pressure gradients were set as the boundary conditions for solid walls. Besides, all walls in the domain were assigned as smooth walls. The realizable k- ϵ turbulence model [26] (variant of the standard k- ϵ model) was chosen to model turbulence quantities. In comparison to other k- ϵ and Spalart-Allmaras turbulence models, the realizable k- ϵ model was used in the simulations due to its stability during computations and accuracy over a wide range of operating conditions [27-29]. Besides, the realizable k- ϵ model was found to give a good agreement between computational and measured performance of VAWT [10, 30]. In addition, it has been considered a proper choice when investigating boundary layer flows under strong adverse pressure gradients or with separation [31]. The realizable k- ϵ model uses the same turbulent kinetic energy equation, k, as the standard k- ϵ model [25], but it has a modified equation for the energy dissipation rate, ϵ . Moreover, the coefficient C_μ (used in the calculation of turbulent

viscosity) is no longer constant as compared to the standard k- ϵ model [32]. A solution convergence tolerance of 10^{-6} was assigned to the simulations. For near wall modelling, the center of the near wall cell (wall-adjacent cells) should be located out of the buffer zone.

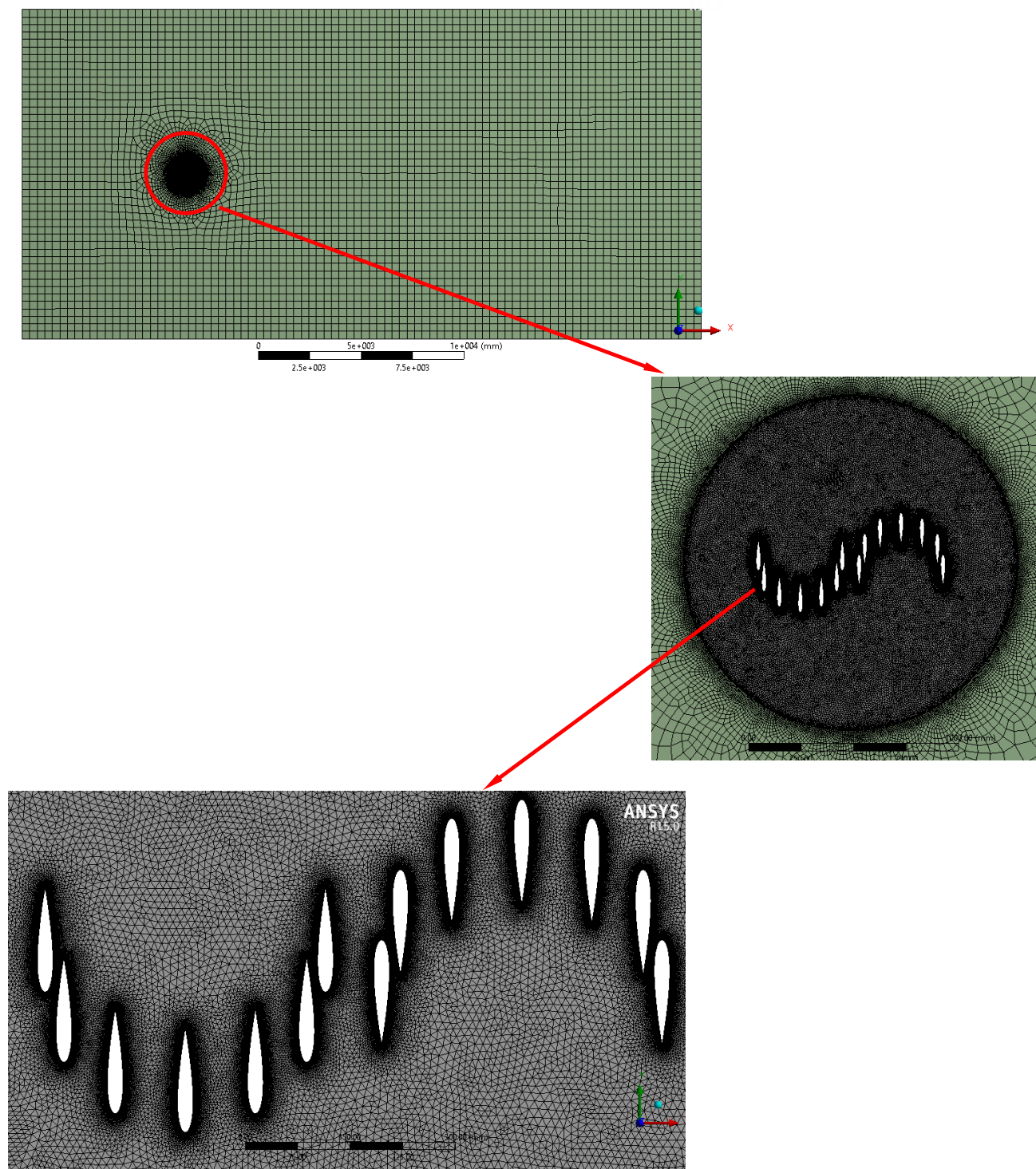


Fig. 7. 2-D Mesh configuration for the H-Darrieus-based integrating wind turbine (State 5 of Figure 5) with mesh details close to blades

4. Wind Turbine Performance Parameters

The main role of the wind turbine rotor blades is to convert the kinetic energy available in the wind stream into mechanical energy in the form of rotational motion of the turbine shaft. The performance of the wind turbine is governed by a set of equations mentioned thereafter.

The theoretical power available in the wind (P_W) is given by the rate of change of wind kinetic energy.

$$P_W = \frac{1}{2} \rho A_s V^3 \quad (4)$$

where ρ is the air density (1.225 kg/m^3), A_s is the rotor swept area of blades and V is the wind speed.

The power extracted from the wind by the turbine (rotor power P_R) is given as:

$$P_R = \omega T \quad (5)$$

where ω is the turbine angular velocity and T is the torque produced by the turbine.

The torque and power coefficients (C_m and C_p) of the wind turbine are written respectively as:

$$C_m = \frac{4T}{\rho A_s V^2 D} \quad (6)$$

$$C_p = \frac{P_R}{P_W} = \frac{2\omega T}{\rho A_s V^3} \quad (7)$$

The tip speed ratio, λ , of the wind turbine is a dimensionless parameter defined so far as the ratio between the tip speed of the rotor blade (ωR) and wind speed (V). It is obtained by the relation:

$$\lambda = \frac{\omega R}{V} \quad (8)$$

where R is the rotor radius ($=D/2$).

Using Eq. (6)-(8), the power coefficient (C_p) can then be rewritten as:

$$C_p = \lambda C_m \quad (9)$$

5. Computational Results and Discussion

In this section, the CFD model will be verified in order to ensure the validity of CFD results. Subsequently, the performance of the Savonius-Darrieus integrating wind turbine will be discussed.

5.1 Verification of CFD Model

A sensitive analysis of grid resolution was made in order to ensure grid independency of the computational results. The grid independence analysis was performed with regards to different configurations of rotor blades orientation shown in Figure 5. The analysis compared the computational results of temporal torque coefficient of four different grid resolutions for each rotor blades configuration. For the H-Darrieus blade configuration (State 5 of Figure 5), for example, the computational domain has the following number of cells for each grid; 304,105 (Grid I), 501,134 (Grid

II), 747,334 (Grid III) and 942,181 (Grid IV). The CFD time and computational resources are noticeably increasing as the mesh density increases.

The CFD results for the four different grids presented in Figure 8 are for the H-Darrieus blade configuration (State 5 of Figure 5) and they were obtained at a wind speed of 10 m/sec and $\lambda = 1$. The results represent a comparison of temporal variations over a complete rotational cycle of Darrieus-based integrating wind turbine torque coefficient for different mesh resolutions. The CFD results were revolution independence. Individually, as illustrated in Figure 8, the torque on the rotor blades depends on the angular position of the blades from the center of rotation. The torque on the rotor is positive when the lift force is dominating and becomes negative due to the drag force on the blades. The resulting cyclic average computational torque coefficient for different grid resolutions respectively are 1.312428, 1.204051, 1.0 and 0.838556 with reference to the one for Grid III. As shown in Figure 8, there is a fairly good agreement between the computational results of mesh resolutions for Grid III and Grid IV. Besides, the deviation in CFD results for different grids mainly appears at the region next to the peak values of torque coefficient. With regards to CFD time, the mesh resolution for Grid III (grid with 747,334 elements) is believed adequate to give grid-independence results.

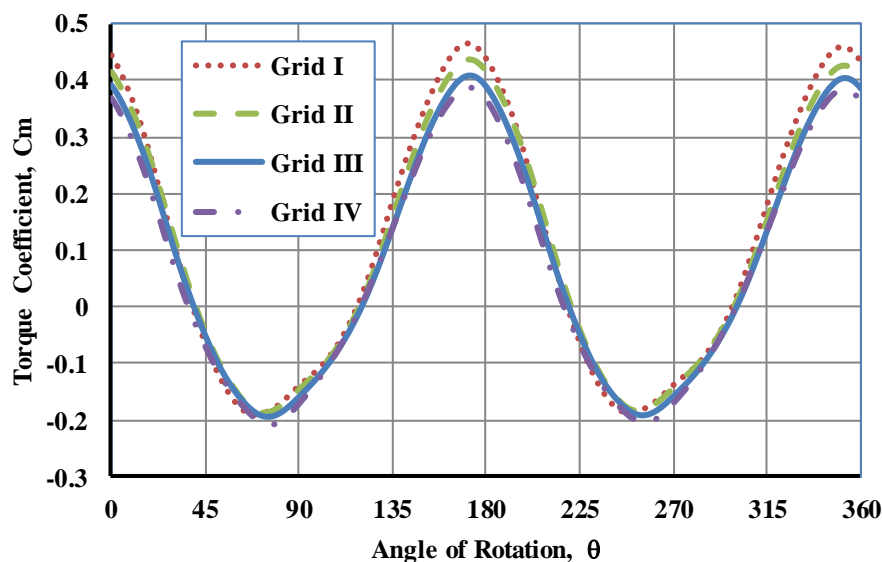


Fig. 8. Grid-independence study results as temporal variation of torque coefficient of different grid resolutions for the Darrieus-based integrating wind turbine. Inlet wind speed = 10 m/sec and $\lambda = 1.0$

5.2 Performance of Savonius-Darrieus Integrating Wind Turbine

Considering the aerodynamics of NACA0015 airfoil, the drag, lift and total forces varies according to the angle of attack (α), see Figure 9 [33]. The drag force is the blade total force in the direction of wind, while the lift force is the one in the perpendicular direction to the wind. At zero-degree angle of attack ($\alpha=0.0$), the upper and lower surfaces of NACA0015 exhibit the same pressure profile and at this condition of the airfoil there is only a drag force. Increasing the angle of attack will modify the pressure distribution on the upper surface. This continues till separation of flow occurs [34-35], which is believed responsible for inducing noise emissions [36]. Uneven distribution of pressure on both surfaces of the airfoil considerably modifies the drag, lift and moment coefficient of the airfoil.

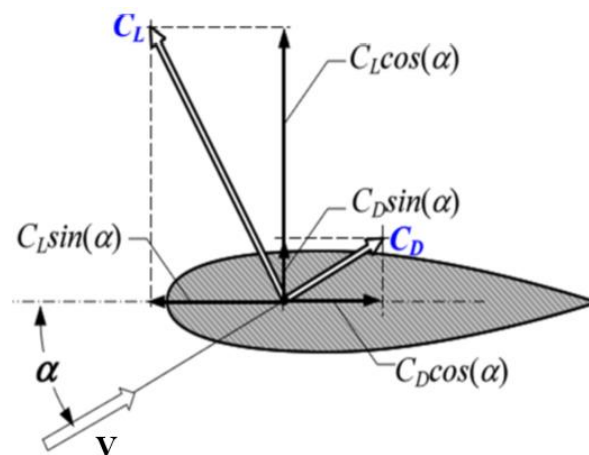


Fig. 9. Lift and drag coefficients (C_L and C_D) of forces acting on blade element; α is the angle of attack [33]

The computational performance of the integrating Savonius-Darrieus wind turbine in terms of cyclic average torque and power coefficients against tip speed ratio is shown in Figure 10. According to the orientation of rotor blades depicted in Figure 5, six rotor configurations (or states) were computationally studied; 0% (State 1 or Savonius State), 25% (State 2), 50% (State 3), 75% (State 4), 100% (State 5 or H-Darrieus State) of blades' full range of regulation, as well as blade chord normal to radial arm (State 6) rotor blade configurations.

As seen in Figure 10, the cyclic average torque and power coefficients are significantly affected by the blade orientation. As illustrated, Savonius based integrating wind turbine (State 1) exhibits lower power coefficient and operates at lower values of λ , but with efficient operation at lower levels of λ as compared to other states. The maximum λ is less than 1 which demonstrates that Savonius cannot revolve faster than the wind as the returning blades (blades in opposition to the wind) cannot travel faster than the wind. When closing flow passages between rotor blades, a Savonius like C-arc blade configuration is formed. This would increase the direct impact of wind with turbine rotor blades (i.e. drag force driven turbine) resulting in high torque coefficient at lower values of tip speed ratio, λ . Switching to the H-Darrieus based integrating wind turbine (State 5), by rotating the rotor blades of State 1 clockwise about their pivots by the full range of blades' angle of adjustment, modifies the performance of the Savonius wind turbine. This increases the peak power coefficient and enables the turbine to run at higher values of λ and consequently at higher rotational speeds, which is considered as a performance gain for Savonius VAWT. In this case the blade chords lines of action are parallel to each other and perpendicular to blades' semicircle diameter.

Regulating the blades' angle between State 1 (Savonius) and State 5 (Darrieus) would generally have a positive effect on turbine performance except for the case with the 25% of full range of adjustment (State 2). Slightly opening the flow passage between rotor blades (State 2) results in a reduction in turbine performance as compared to State 1 (Savonius State). This may be attributed to the lower pressure created in front of blades. With a continuous increase in the degree of angle of adjustment of rotor blades in clockwise direction, a significant modification in turbine performance takes place. Among the investigated cases, the highest peak power coefficient with a wide range of λ was obtained through partial opening of flow passages between rotor blades with configuration for State 4, see Figure 5(d). This can be accomplished by making the flow passage between rotor blades of the H-Darrieus based integrating wind turbine 75% of full range of regulation, but with

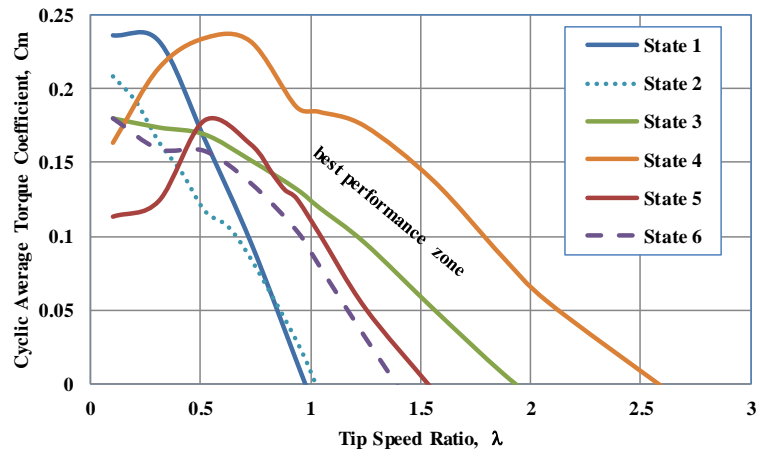
uneven orientation of individual blades. Tuning rotor blades orientation might not result in any further improvements in turbine performance than the 75% case (State 4).

Thus, managing blades orientation or the flow passages between rotor blades could significantly affect the resulting lift force and consequently the turbine output power. Controlling the flow gaps between individual blades by regulating the rotor blades of State 1 around their pivots would vary the resulting torque where the turbine is being driven by lift force (i.e. lift force driven). The produced summing torque depends on the angle of attack of individual rotor blades, which in turn differs from one blade to another as well as it is in continuous variation during rotation of turbine rotor. This means that the resulting instantaneous torque may either be greater or smaller than the corresponding one in the case where flow passages are fully close (i.e. Savonius like configuration).

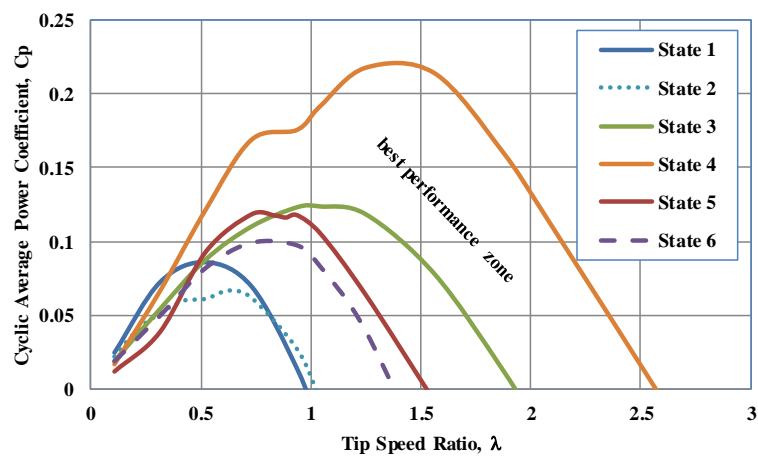
Accordingly, managing the flow passages between rotor blades, by adjusting blade orientation, would control the wind turbine performance. The wind turbine, therefore, would have potential to work at high tip speed ratios with higher power coefficient. Optimum performance of the proposed integrating turbine design is believed to be obtained within the region bounded by the performance curves of State 1, State 5, State 3 and State 4 (best performance zone in Figure 10). It has to be clarified that the size (or dimensions) of turbine rotor would considerably affect the degree of interference of various performance curves and consequently the operating range of tip speed ratio λ . Besides, proper selection of rotor turbine dimensions as well as overlapping ratio of rotor blades would help in magnification of turbine output power to match well with those shown in Figure 2. Turbine dimensions may include blades' semicircle radius, size of airfoil blade and arrangement of airfoils on blades' semicircle.

Figure 11 compares the time-based torque coefficient over a complete cycle of rotation for various states of rotor blades at $\lambda = 0.7$; where performance curves for all states under investigation are within the operating range. In this figure, the rotor angle 0° corresponds to the positions of rotor blades shown in Figure 5. As depicted, the angle at which the torque coefficient represents either a peak or a trough value depends on rotor blades configuration. This means that there is a phase difference between peaks and troughs of different configurations. Blades orientation for State 5 (Darrieus State) exhibits a torque coefficient curve with the highest peaks and lowest troughs and with a steep gradient, which in turn reduces the cyclic average torque coefficient at this condition. Curves with lower peaks (State 2 for instance) have lower values of average torque coefficient. Uneven orientation of rotor blades results in multiple ripples on various curves as well as unequal starting torques. Regardless the average value of cyclic torque coefficient, it is observed that State 1, State 2 and State 5 are the only states at this value of λ that produce negative torque.

Comparisons of pressure coefficient contours at $\lambda = 0.7$ for different rotor blades configurations are illustrated in Figure 12. The pressure coefficient is defined as the ratio between the local static pressure and the dynamic pressure of the wind at the free upstream end. The contours are temporally displayed within the zone surrounding the turbine rotor, i.e. the rotating zone, at rotor angles of 0° , 45° , 90° and 135° . Regions with high pressure coefficient are colored in red while regions with low pressure coefficient are colored in blue. The behavior of pressure coefficient is that the maximum value is generally increasing till rotor angle of 90° and then it decreases. The percentage increase in the value of maximum pressure coefficient from 0° to 45° rotor angle is always less than that from 45° to 90° . The Savonius rotor configuration (State 1) exhibits lower values of maximum pressure coefficient as compared to other states. As depicted, managing gaps between rotor blades may result in more negative pressure when compared to State 1.



(a) Cyclic average torque coefficient, C_m , versus tip speed ratio, λ



(b) Cyclic average power coefficient, C_p , versus tip speed ratio, λ

Fig. 10. Variation of CFD cyclic average (a) torque and (b) power coefficients of the proposed integrating wind turbine design with tip speed ratio. States 1 to 6 are illustrated in Figure 5

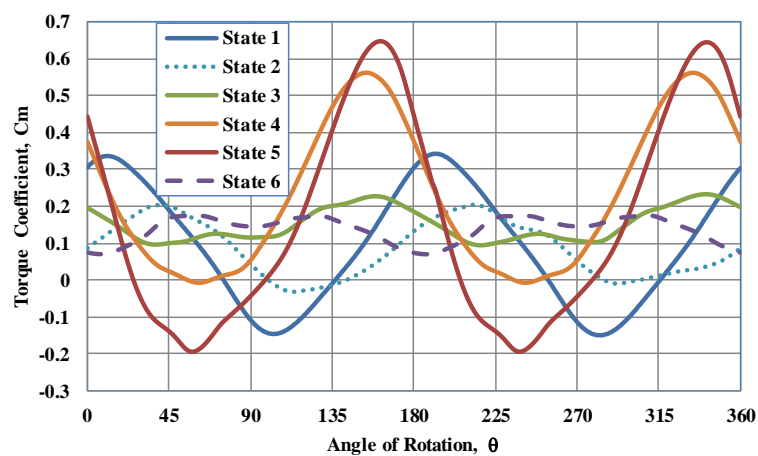


Fig. 11. Comparison of instantaneous torque coefficient for various rotor blade configurations at $\lambda = 0.7$

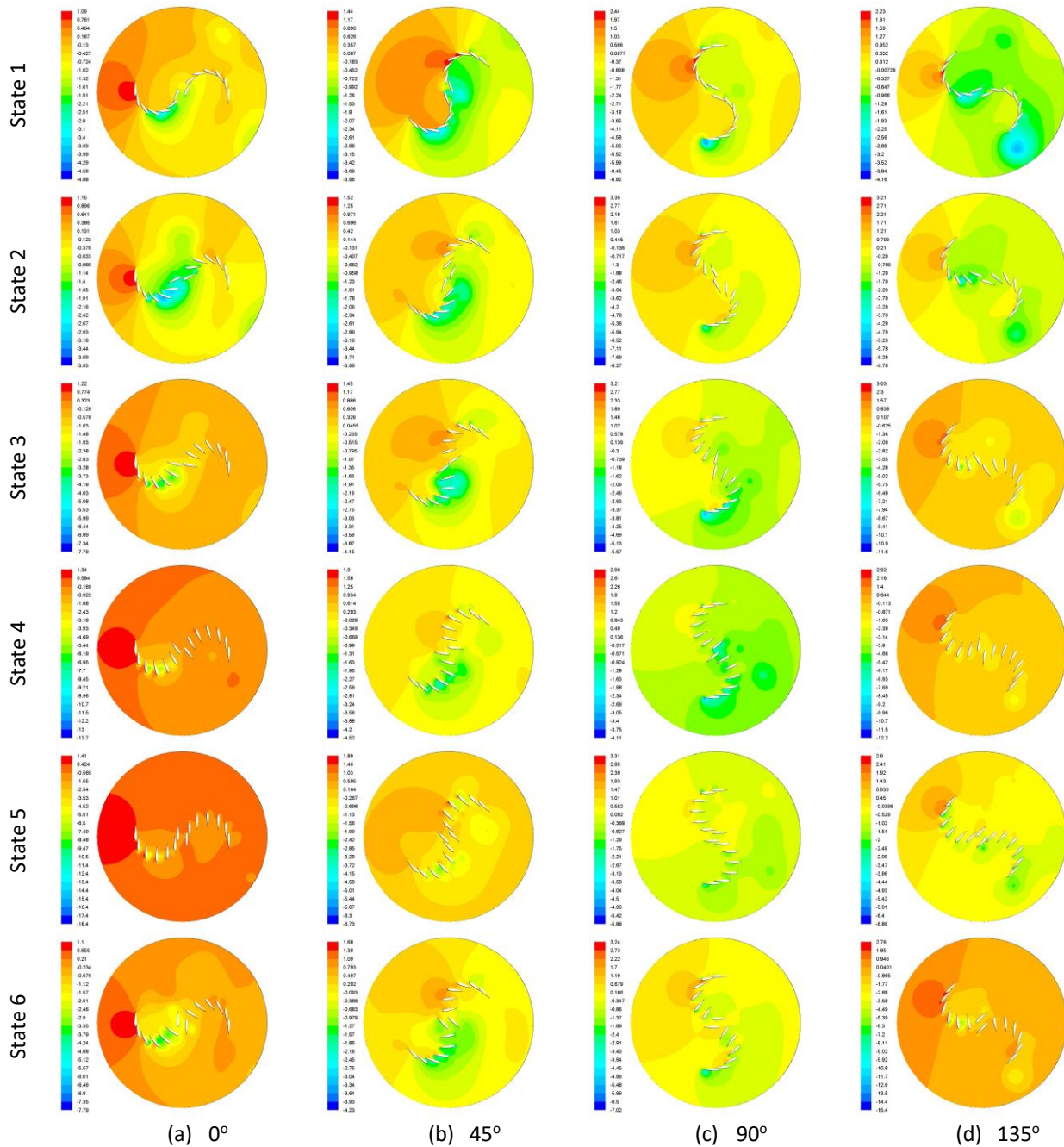


Fig. 12. Comparisons of pressure coefficient contours for various rotor blade configurations at $\lambda = 0.7$ and rotor angles of (a) 0° , (b) 45° , (c) 90° and (d) 135°

6. Conclusions

In this paper, a Computational Fluid Dynamics investigation of a novel design configuration of a Vertical Axis Wind Turbine (VAWT) was carried out. The objective was to take the advantages of both of Savonius and Darrieus types of VAWT in a single non-hybrid design. The proposed design is an integrating design of both of Savonius and H-Darrieus wind turbines in a one configuration. In this design, the turbine rotor consists of a few similar NACA0015 airfoil blades arranged particularly for this purpose. By adjusting individual angles of rotor blades, the turbine would operate either as Savonius or H-Darrieus VAWT. Some state configurations of rotor blades were suggested as test cases for the computational study based on blades' angle of regulation. Each rotor design was

computationally investigated to determine its performance as well as the operating range of tip speed ratio. The computational results showed that the performance parameters of the proposed design are significantly affected by rotor blades orientation. Besides, CFD results suggest a considerable improvement in the performance of Savonius VAWT when applying this design. The new design would help switching between the two designs (Savonius and H-Darrieus) and thus covers the operating range of performance parameters between both types of wind turbines. The performance of the proposed wind turbine could be optimized and easily managed through the adjustment of rotor blades. In a work to follow, this study will be to optimize the integrating turbine performance in terms of turbine dimensions, airfoil blade shape and dimensions, number of airfoil blades, and arrangement of airfoils on blades' semicircle.

Acknowledgements

The author would like to thank Prof. Nagy I. Elkalashy, Department of Electrical Engineering, Menoufiya University, for his invaluable guidance, support and discussions.

References

- [1] Eriksson, Sandra, Hans Bernhoff, and Mats Leijon. "Evaluation of different turbine concepts for wind power." *renewable and sustainable energy reviews* 12, no. 5 (2008): 1419-1434.
<https://doi.org/10.1016/j.rser.2006.05.017>
- [2] Damak, A., Z. Driss, and M. S. Abid. "Experimental investigation of helical Savonius rotor with a twist of 180." *Renewable Energy* 52 (2013): 136-142.
<https://doi.org/10.1016/j.renene.2012.10.043>
- [3] Roy, Sukanta, and Ujjwal K. Saha. "Wind tunnel experiments of a newly developed two-bladed Savonius-style wind turbine." *Applied Energy* 137 (2015): 117-125.
<https://doi.org/10.1016/j.apenergy.2014.10.022>
- [4] Lee, Jae-Hoon, Young-Tae Lee, and Hee-Chang Lim. "Effect of twist angle on the performance of Savonius wind turbine." *Renewable Energy* 89 (2016): 231-244.
<https://doi.org/10.1016/j.renene.2015.12.012>
- [5] El-Askary, W.A., Ahmed S. Saad, Ali M. AbdelSalam, and I.M. Sakr. "Investigating the performance of a twisted modified Savonius rotor." *Journal of Wind Engineering and Industrial Aerodynamics* 182 (2018): 344-355.
<https://doi.org/10.1016/j.jweia.2018.10.009>
- [6] Chan, C.M., H.L. Bai, and D.Q. He. "Blade shape optimization of the Savonius wind turbine using a genetic algorithm." *Applied Energy* 213 (2018): 148-157.
<https://doi.org/10.1016/j.apenergy.2018.01.029>
- [7] Zhang, Baoshou, Baowei Song, Zhaoyong Mao, Wenlong Tian, Boyang Li, and Bo Li. "A Novel Parametric Modeling Method and Optimal Design for Savonius Wind Turbines." *Energies* 10 (2017): 301.
<https://doi.org/10.3390/en10030301>
- [8] El-Askary, W.A., M.H. Nasef, A.A. AbdEL-hamid, and H.E. Gad. "Harvesting wind energy for improving performance of Savonius rotor." *Journal of Wind Engineering and Industrial Aerodynamics* 139 (2015): 8-15.
<https://doi.org/10.1016/j.jweia.2015.01.003>
- [9] Korprasertsak, Natapol, and Thananchai Leephakpreeda. "Analysis and optimal design of wind boosters for Vertical Axis Wind Turbines at low wind speed." *Journal of Wind Engineering and Industrial Aerodynamics* 159 (2016): 9-18.
<https://doi.org/10.1016/j.jweia.2016.10.007>
- [10] Mohamed, M.H., G. Janiga, E. Pap, and D. Thévenin. "Optimal blade shape of a modified Savonius turbine using an obstacle shielding the returning blade." *Energy Conversion and Management* 52, no. 1 (2011): 236-242.
<https://doi.org/10.1016/j.enconman.2010.06.070>
- [11] Wenehenubun, Frederikus, Andy Saputra, and Hadi Sutanto. "An experimental study on the performance of Savonius wind turbines related with the number of blades." *Energy Procedia* 68 (2015): 297-304.
<https://doi.org/10.1016/j.egypro.2015.03.259>
- [12] Sranpat, Chaianant, Suchaya Unsakul, Premchai Choljararux, and Thananchai Leephakpreeda. "CFD-based performance analysis on design factors of vertical axis wind turbines at low wind speeds." *Energy Procedia* 138 (2017): 500-505.
<https://doi.org/10.1016/j.egypro.2017.10.235>

- [13] Jian, Chen, Jan Kumbertuss, Zhang Linhua, Lu Lin, and Yang Hongxing. "Influence of Phase-Shift and Overlap Ratio on Savonius Wind Turbine's Performance." *ASME Journal of Solar Energy Engineering* 134 (2012): 011016-1.
<https://doi.org/10.1115/1.4004980>
- [14] Alam, Md Jahangir, and Mohammad T. Iqbal. "Design and development of hybrid vertical axis turbine." In *2009 Canadian Conference on Electrical and Computer Engineering*, pp. 1178-1183. IEEE, 2009.
<https://doi.org/10.1109/CCECE.2009.5090311>
- [15] Zakaria, Ahmad, and Mohd Shahrul Nizam Ibrahim. "Velocity Pattern Analysis of Multiple Savonius Wind Turbines Arrays." *CFD Letters* 12, no. 3 (2020): 31-38.
<https://doi.org/10.37934/cfdl.12.3.3138>
- [16] Wong, Kok Hoe, Wen Tong Chong, Nazatul Liana Sukiman, Yui-Chuin Shiah, Sin Chew Poh, Kamaruzzaman Sopian, and Wei-Cheng Wang. "Experimental and simulation investigation into the effects of a flat plate deflector on vertical axis wind turbine." *Energy Conversion and Management* 160 (2018): 109-125.
<https://doi.org/10.1016/j.enconman.2018.01.029>
- [17] Ali, Mohammed Hadi. "Experimental Comparison Study for Savonius Wind Turbine of Two & Three Blades At Low Wind Speed." *International Journal of Modern Engineering Research* 3, no. 5 (2013): 2978-2986.
- [18] Ahmedov, Ahmed. "Investigation of the performance of a hybrid wind turbine Darrieus-Savonius." PhD diss., Loughborough University, 2016.
- [19] Hosseini, Arian, and Navid Goudarzi. "Design and CFD study of a hybrid vertical-axis wind turbine by employing a combined Bach-type and H-Darrieus rotor systems." *Energy Conversion and Management* 189 (2019): 49-59.
<https://doi.org/10.1016/j.enconman.2019.03.068>
- [20] Hau, Erich. *Wind Turbines: Fundamentals, Technologies, Application, Economics*. Springer, Germany, 2006.
- [21] Ragheb, Magdi, and Adam M. Ragheb. "Wind turbines theory-the betz equation and optimal rotor tip speed ratio." *Fundamental and advanced topics in wind power* 1, no. 1 (2011): 19-38.
<https://doi.org/10.5772/21398>
- [22] <http://airfoiltools.com/airfoil/details?airfoil=naca0015-il>. Accessed in March 2019.
- [23] Yi, Mei, Qu Jianjun, and Li Yan. "Airfoil design for vertical axis wind turbine operating at variable tip speed ratios." *The Open Mechanical Engineering Journal* 9, no. 1 (2015).
<https://doi.org/10.2174/1874155X01509011007>
- [24] ANSYS Fluent. "Fluent 15.0 User's Guide." *Fluent Incorporated*, Lebanon, NH, (2015).
- [25] Launder, B.E., and D.B. Spalding. "The Numerical Computation of Turbulent Flows." *Computer Methods in Applied Mechanics and Engineering* 3 (1974): 269-289.
[https://doi.org/10.1016/0045-7825\(74\)90029-2](https://doi.org/10.1016/0045-7825(74)90029-2)
- [26] Shih, Tsan-Hsing, William W. Liou, Aamir Shabbir, Zhigang Yang, and Jiang Zhu. "A New k- ϵ Eddy-Viscosity Model for High Reynolds Number Turbulent Flows." *Computers and Fluids* 24, no. 3 (1995): 227-238.
[https://doi.org/10.1016/0045-7930\(94\)00032-T](https://doi.org/10.1016/0045-7930(94)00032-T)
- [27] Shahzad, Atif, Taimoor Asim, Rakesh Mishra, and Achilleos Paris. "Performance of a Vertical Axis Wind Turbine under Accelerating and Decelerating Flows." *Procedia CIRP* 11 (2013): 311-316.
<https://doi.org/10.1016/j.procir.2013.07.006>
- [28] Liang, Xiaoting, Sauchung Fu, Baoxing Ou, Chili Wu, Christopher Y.H. Chao, and Kaihong Pi. "A computational study of the effects of the radius ratio and attachment angle on the performance of a Darrieus-Savonius combined wind turbine." *Renewable energy* 113 (2017): 329-334.
<https://doi.org/10.1016/j.renene.2017.04.071>
- [29] Roy, Sukanta, and Ujjwal K. Saha. "Comparative analysis of turbulence models for flow simulation around a vertical axis wind turbine." In *Indo-Danish International Conference on Wind Energy: Materials, Engineering, and Policies (WEMEP 2012)* (2012).
- [30] Saeed, Hassan A. Hassan, Ahmed M. Nagib Elmekawy, and Sadek Z. Kassab. "Numerical study of improving Savonius turbine power coefficient by various blade shapes." *Alexandria Engineering Journal* 58 (2019): 429-441.
<https://doi.org/10.1016/j.aej.2019.03.005>
- [31] Srinivasan, G.R., J.A. Ekaterinaris, and W.J. McCroskey. "Evaluation of turbulence models for unsteady flows of an oscillating airfoil." *Computers and Fluids* 24 (1995): 833-861.
[https://doi.org/10.1016/0045-7930\(95\)00016-6](https://doi.org/10.1016/0045-7930(95)00016-6)
- [32] Obeid, Sohaib, Ratneshwar Jha, and Goodarz Ahmadi. "RANS Simulations of Aerodynamic Performance of NACA 0015 Flapped Airfoil." *Fluids* 2, no. 2 (2017).
<https://doi.org/10.3390/fluids2010002>
- [33] Tchakoua, Pierre, René Wamkeue, Mohand Ouhrouche, Tommy Andy Tameghe, and Gabriel Ekemb. "A New Approach for Modeling Darrieus-Type Vertical Axis Wind Turbine Rotors Using Electrical Equivalent Circuit Analogy: Basis of Theoretical Formulations and Model Development." *Energies* 8 (2015): 10684-10717.

<https://doi.org/10.3390/en81010684>

- [34] Miller, Steven D. "Lift, Drag and moment of a NACA 0015 Airfoil." *Department of Aerospace engineering* 28 (2008).
- [35] Bangga, Galih, Thorsten Lutz, Amgad Dessoky, and Ewald Kramer. "Unsteady Navier-Stokes studies on loads, wake, and dynamic stall characteristics of a two-bladed vertical axis wind turbine." *Journal of Renewable and Sustainable Energy* 9, no. 5 (2017): 053303.
<https://doi.org/10.1063/1.5003772>
- [36] Dessoky, Amgad, Thorsten Lutz, Galih Bangga, and Ewald Kramer. "Computational studies on Darrieus VAWT noise mechanisms employing a high order DDES model." *Renewable Energy* 143 (2019): 404-425.
<https://doi.org/10.1016/j.renene.2019.04.133>